LEADING EDGE VORTEX SYSTEM OF THE A380 AT HIGH ANGLES OF ATTACK IN LANDING CONFIGURATION

R. Emunds,
Airbus Operations GmbH, Airbusallee 1, 28199 Bremen, Germany

Abstract

Maximum lift for commercial transport aircraft is naturally limited by the very complex flow field in the junction of the wing and the nacelle. This geometrical area can be characterized by the interaction of several shear layers and vortex systems which are subjected to the global wing pressure field when travelling downstream over the wing suction surface.

The current contribution deals with the development of the nacelle / pylon / wing shear layers and vortex systems of the A380 landing configuration based on 3D Computational Fluid Dynamics (CFD). Special focus is put on the origin of the different shear layer systems building up at the inner pylon and the inner nacelle developing into interacting vortex systems at increasing angles of attack.

1. INTRODUCTION

Prediction of maximum lift or maximum achievable angle of attack (AoA) for modern commercial transport aircrafts is still a very challenging issue for today's CFD tools. In industry, current practice is based on 3D steady state numerical solvers utilizing structured and hybrid grids depending on the geometrical complexity of the problem to be investigated. Although the prediction of maximum lift and maximum angle of attack cannot be done in a quantitative manner today, CFD allows a deep insight into the flow physics leading to wing stall. Thus, today's CFD method is capable of predicting qualitatively the correct physical mechanisms, but usually at far too low angles of attack. Current research programs like HINVA (LuFo IV) are intended to provide inputs for improving the prediction capabilities in the future [2].

2. NUMERICAL SETUP

The current investigation has been performed using the DLR TAU Code [1]. TAU is a compressible flow solver based on an unstructured finite volume scheme. Inviscid fluxes are discretized by central differences with artificial dissipation. Viscous fluxes are also discretized centrally. Turbulence is handled for the current investigation by the 2-eqn. Menter SST model [3] and the turbulent convective terms are resolved by a second order ROE scheme. Time marching is done using a semi-implicit lower-upper Gauss-Seidel scheme (LU-SGS). Multigrid convergence acceleration is applied by a 3w cycle for the main conservation equations.

The underlying numerical grid used for the current study is generated using the commercial grid generator CENTAUR [4]. The first wall distance is defined according to the A/C Reynolds-number as 2e-6m leading to a non-dimensional wall distance y+ lower than one everywhere on the A/C surface. Certain local grid refinement areas are specified to allow a proper prism growth and to allow for good resolution of free vortices. According to the latter, and especially to resolve the nacelle strake vortices properly, strong grid refinement is applied downstream of the nacelle strakes in the area of the expected vortex path. This global grid refinement is also sufficient to resolve the weaker vortex structure like nacelle vortices and pylon shoulder vortices. The final grid used in the current study has about 72Mio nodes; only a half model is considered due to symmetry of the A/C. Figure 1 depicts the surface grid and the y+ distribution for an AoA in the upper linear range of the lift polar.

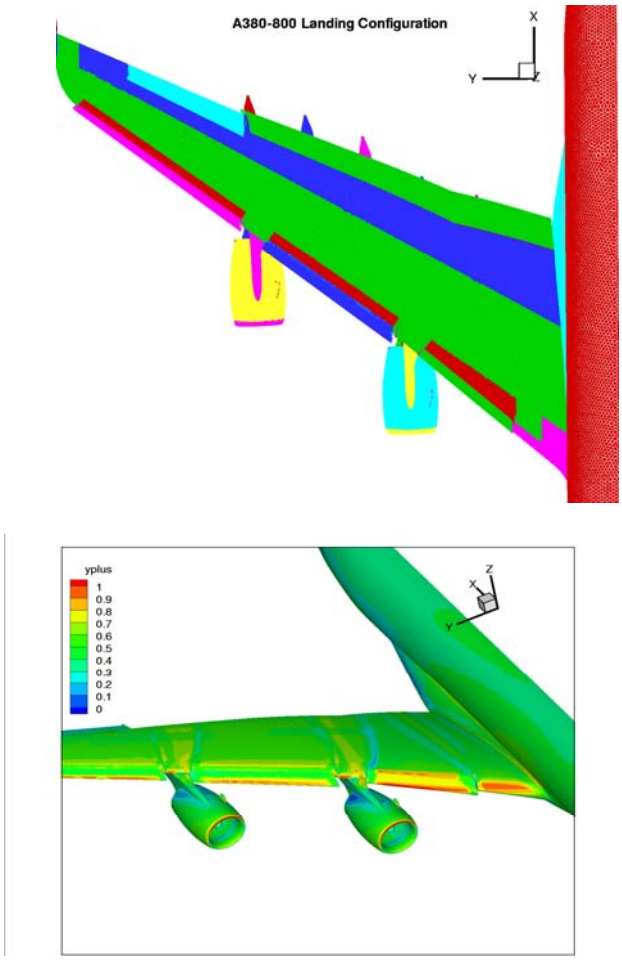

Figure 1: Surface Grid and Y+ Distribution

3. RESULTS

The presentation of the results is done, based on a comparison between the predicted lift polar plus predicted surface flow features and available windtunnel data followed by a detailed analysis of the wing leading edge / nacelle / pylon flow physics.

3.1. Comparison CFD vs. WTT

Figure 2 compares the predicted lift polar with available WTT data (ONERA-F1-LSWT). For the computation, flight Re-number has been assumed. Two different CFD results are shown only differing in the applied artificial viscosity scheme. As can be seen, both predictions miss the upper range of the polar; the result based on so-called Matrix Dissipation is superior to the one with Scalar Dissipation. In addition, in the lower AoA regime, an offset in comparison to the WTT data is present. The latter is related to a flap flow found as being unsteady in the experiment. This unsteady flow behavior is predicted by CFD as a local flow separation leading to a reduced circulation and thus to a reduction in configuration lift. For increasing AoA this flow unsteadiness along the flap vanishes and so does the separation in the CFD prediction. Thus for the middle portion of the linear polar range the computation moves towards the experimental result. For the higher linear AoA region, the flow in the experiment shows some unsteady behavior downstream of the pylon / wing intersection which is finally computed as a separation in CFD, which in consequence defines the predicted maximum AoA. The flow physics developing in the pylon / wing junction area, leading to the observed unsteadiness is the subject of the second part of this chapter.

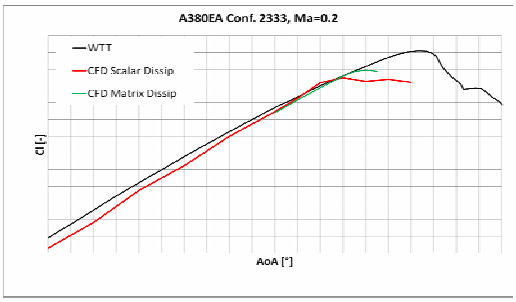

Figure 2: Lift Polar: CFD vs. WTT

Figure 3 shows a comparison between the suction surface flow field for CFD and WTT for two angles of attack in the upper linear range of the polar. For the lower AoA (Top row in Figure 3) the tufts indicate the active flow regime developing downstream of the pylon / wing junction. The occurring crossflow is captured well by the CFD computation. Increasing the AoA by about 1° leads to the result shown in the bottom row of Figure 3. The unsteady flow behavior downstream of the pylon / wing junction is strengthened in the experiment while the CFD result shows already the tendency of flow separation. The AoA corresponds to the maximum lift predicted by the CFD result.

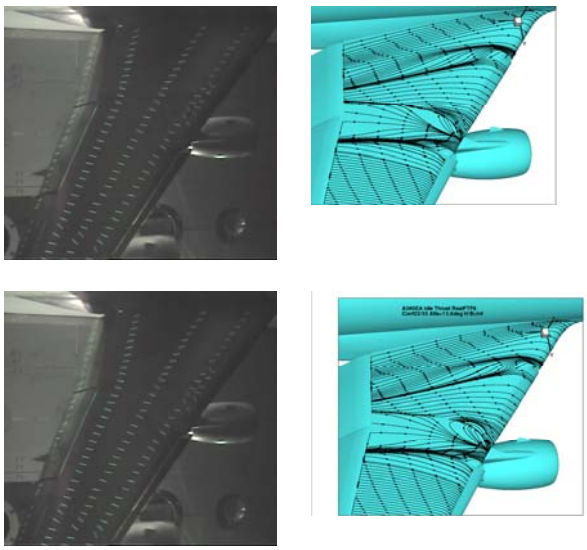

Figure 3: Comparison CFD vs. WTT for two AoA's in the upper linear polar range

3.2. Wing / Pylon junction flow physics

The complex flow structure present in the pylon / wing junction will be looked at in this chapter based on streamline distributions on the pylon, the nacelle and the wing suction surface. In addition, the various vortices are visualized by the ratio of the strain rate tensor S_{ij} and the rotational tensor Ω_{ij}.

Due to the wing sweep angle, a spanwise outboard flow is present along the Droopnose Device (DND). The footprint of this flow on the inner engine pylon sidewall is clearly visible by the bluff body like streamline distribution. On the nacelle rear part, the footprint of a structure is visible which represents the development of some 3D flow separation. For lower AoA a strong flow is present along the nacelle which follows the nacelle contour towards its intersection with the engine pylon. For higher AoA (as shown in Figure 4) the nacelle flow and the pylon flow start interacting with each other. For the currently considered AoA the strong nacelle flow makes the flow running down the pylon separating, yielding a vortex footprint as marked in the figure as *nacelle separation vortex footprint*. This vortex is more easily seen in the bottom picture of Figure 4, which visualizes the vortex in the volume. Based on the strong negative pressure coefficient present at the DND leading edge, the remaining pylon shear layers as well as the nacelle separation vortex are sucked towards the wing suction surface along the inner pylon inner side wall. When passing further downstream, these structures are met by the DND sidewall vortex and the wing corner vortex. On top of this, the pylon shoulder vortex also travels downstream in this region. The complexity of the resulting vortex systems present in the vicinity of the pylon / wing junction is depicted in the middle picture of Figure 4.

As can be seen by the vortex visualization, certain vortices have already burst in the CFD computation, while others are still present but not predicted to be strong enough to withstand the adverse pressure gradient downstream of the wing leading edge. Based on this predicted vortex burst and based on the too weak remaining vortical

structures, the wing suction surface boundary layer gets artificially weakened resulting in a premature flow separation in the prediction.

At this point, the impact of the nacelle strake vortex needs to be briefly considered. In general, the strong vortical structure generated from the nacelle strake is capable of curing most of the negative effects carried on to the wing suction side from the above mentioned shear layers. Unfortunately, for the A380 landing configuration, the nacelle strake vortex is too far away from the wing to cure the wing suction surface separation due to the early vortex burst described before. In addition, the full strength of the nacelle strake vortex has not yet developed due to the low AoA for which the CFD results predict maximum lift. Besides the nacelle strake vortex strength, its relative position with respect to the pylon / wing junction plays also an important role. Figure 5 shows the location of the different vortices in an x=const plane for two AoA. Colouring represents streamwise velocity. Two well established vortices can be found at first glance: the nacelle strake vortex and the nacelle vortex. The latter is rotating clockwise while the nacelle strake vortex turns counter-clockwise. Comparing the two pictures in Figure 5 it can be seen, that a 1degree increase in AoA leads to a strong change in the pylon / wing junction velocity field. The area of low streamwise velocity enlarges quickly, while the nacelle strake vortex impact has not really changed. From the computation, the spanwise position of the nacelle strake vortex is for the considered AoA still too far away from the pylon / wing junction to cure any flow problems.

Various explanations are seen for the under-prediction of vortex strength in the current simulation and thus the mismatch of predicted maximum AoA and measured one. Firstly, it is known that the applied turbulence model out of the eddy viscosity model class is not able to predict the correct pressure distribution in the vortex core resulting in premature vortex breakdown. Secondly, the artificial viscosity scheme seems to impact the vortex development as could be seen by the higher achievable AoA when applying the Matrix Dissipation scheme. Thirdly, the very complex geometrical situation in the pylon / wing junction is very challenging for the grid generator. Although prism chopping could widely be avoided during the grid generation process, pullback of the prisms could not. Unfortunately, the current version of CENTAUR does not allow for an insertion of a structured grid portion in this area which is seen as being very favourable with respect to vortex convection. Finally, the experimentally observed local unsteadiness downstream of the pylon / wing junction might limit the applicability of steady state CFD and thus might require an unsteady CFD assessment.

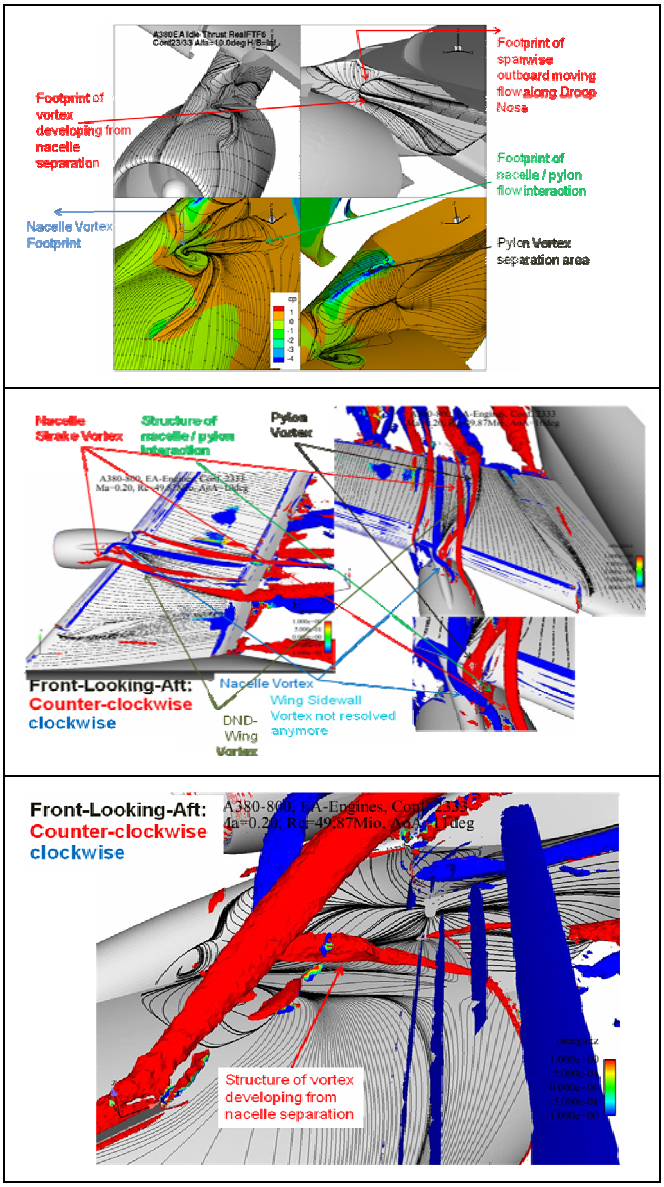

Figure 4: Streamlines and volume vortex visualization of pylon / nacelle / wing area; upper linear AoA area

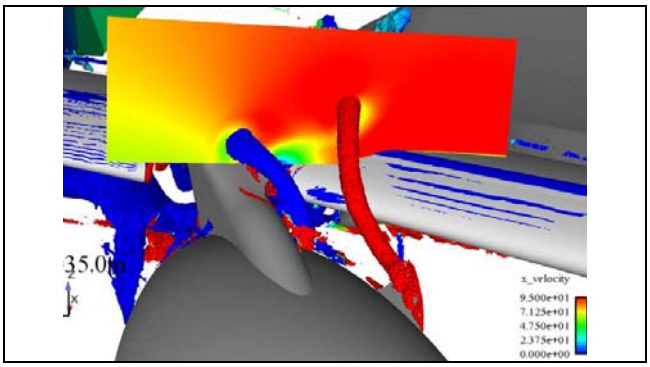

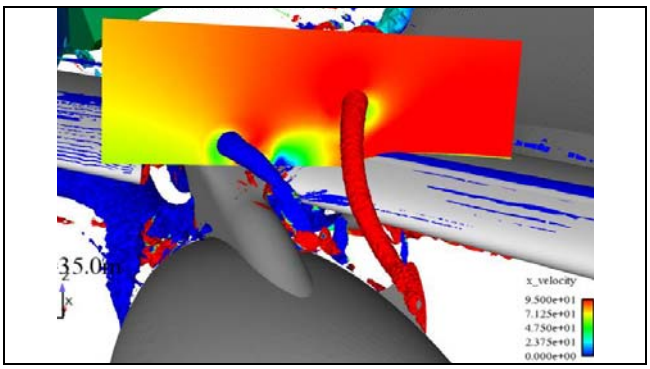

Figure 5: Position of Strake vortex close to CFD α_{max}

4. CONCLUSION

A numerical study has been performed on the A380 landing configuration based on the DLR TAU code with the Menter SST turbulence model. Up to the higher linear range of the polar the predicted results agree quite well with experiments. Comparison of tuft pictures with streamline pictures from CFD shows that the CFD simulation is able to predict the correct flow development leading to stall. With this, valuable insight into the physics yielding stall can be gained. Beside this correct representation of flow phenomena, the correct strength of the vortical flow structures responsible for A/C stall are not captured in the simulation for the higher AoA due to premature vortex burst. The main reason for this is currently seen in the applied turbulence model being a member of the eddy viscosity models. Future work will be done based on differential Reynolds-stress models. As well as the turbulence model, the application of a steady numerical algorithm might also be seen as a reason for premature vortex breakdown. Depending on the outcome of the Reynolds-Stress Model simulations, some thought might be worth spending on unsteady considerations.

5. REFERENCES

[1] **Schwamborn, D.; Gerhold, T.; Heinrich, R. : "***The DLR TAU Code: Recent applications in Research and Industry", European Conf. on CFD, ECOMAS CFD 2006*

[2] **HINVA-Project, "***50th AIAA Aerospace Sciences Meeting including the New Horizons Forum and Aerospace Exposition", 09 - 12 January 2012, Nashville, Tennessee*, *AIAA-2012-0106*

[3] **Menter, F.R.**: "Two Equation Eddy-Viscosity Turbulence Models for Engineering Applications", AIAA Journal 32(8): 1598-1605

[4] www.centaursoft.com, User Manual